

PACS numbers: 42.25.Dd; 42.25.Fx
DOI: 10.1070/QE2007v037n01ABEH013335

On the estimate of effective optical parameters of close-packed fibrillar media

D.A. Zimnyakov, L.V. Kuznetsova, O.V. Ushakova, R. Myllylä

***Abstract*. A method is proposed for determining effective optical parameters of multiply scattering random media by analysing the angular intensity distribution of coherent backscattering from a finite-thickness medium layer taking into account the reflectivity of its boundaries. The optical parameters of dry paper layers and paper layers saturated with immersion liquids are studied in the visible region by measuring the half-widths of coherent backscattering peaks at 633 and 532 nm and using the diffuse and collimated transmission spectroscopy. It is shown that the scattering of probe radiation in paper layers is isotropic.**

Keywords: *multiple scattering, random media, transport length.*

1. Introduction

Optical methods for probing random media are widely used at present in biology, medicine, and materials technology. The probe radiation transfer in objects under study can be described in a number of cases by using the diffusion approximation of the radiation transfer theory [1, 2] which employs the transport scattering coefficient μ_s' and absorption coefficient μ_a as parameters of a medium being probed. The propagation of probe radiation in the medium also considerably depends on the scattering anisotropy parameter g, which is defined as

$$g = \langle \cos\theta \rangle = \frac{\int_0^\pi \cos\theta \sin\theta \, p(\theta) \mathrm{d}\theta}{\int_0^\pi \sin\theta \, p(\theta) \mathrm{d}\theta},$$

where θ is the scattering angle, and the scattering phase function $p(\theta)$ describes the angular intensity distribution of radiation scattered by an isolated scatterer [1]. For close-packed random media, in which correlations of the positions of scattering particles substantially affect the propagation of light, the effective phase function of the medium, calculated taking into account the statistical structural factor of the scattering system, is used as $p(\theta)$ (see, for example, [3, 4]). In the case of polydisperse scattering systems, the parameters μ_s', μ_a, and g are determined by averaging their values over ensembles of scatterers. In the case of weakly absorbing random media ($\mu_s' \gg \mu_a$), the scattering anisotropy parameter determines the relation between two characteristics scales in a random medium being probed – the transport length $l^* = (\mu_s')^{-1}$ and scattering length $l = \mu_s^{-1}$, where μ_s is the scattering coefficient: $l^* = l/(1-g)$ [1].

Within the framework of weak scattering approximation ($\lambda \ll l$), the relation between structural characteristics of a medium being probed (concentration and average size of scattering centres) and transport parameters l, l^* and $l_a = \mu_a^{-1}$ can be found by calculating the scattering (σ_s) and absorption (σ_a) cross sections of scatterers and the value of g (for example, by using the Mie theory [5]) and then determining the scattering length $l = (\sigma_s c)^{-1}$, absorption length $l_a = (\sigma_a c)^{-1}$, and transport length $l^* = [\sigma_s c(1-g)]^{-1}$, where c is the volume concentration of scatterers. From the point of view of optical diagnostics of multiply scattering random media, which are characterised by weak absorption (they include, for example, most of the biological tissues probed in the wavelength range from 0.7 to 1.2 μm), the transport length is an important parameter determining the distance in the medium at which the regime of directional transfer of probe radiation passes to the diffuse propagation regime. The ratio l^*/l also plays an important role in the description of probe radiation transfer in random media because it determines the characteristic number of scattering events required for the stochastisation of the radiation wave vector in the medium. In the case $l^* \gg l$, the medium is characterised by substantial anisotropic scattering of probe radiation, whereas for $l^* \approx l$, isotropic scattering occurs in the medium, which is, as a rule, typical for ensembles of scattering centres of size considerably smaller than the wavelength.

The value of l^* is usually determined by measuring the diffuse transmission T_d of a layer of the medium under study and (or) diffuse reflection R_d from this layer with the help of integrating spheres (see, for example, [6]). The value of l for weakly absorbing media can be found by measuring the collimated transmission T_c from the expression $l \approx W/\ln(1/T_c)$ (where W is the probed layer thickness) taking into account Fresnel reflection losses at the layer boundaries.

D.A. Zimnyakov, L.V. Kuznetsova N.G. Chernyshevsky Saratov State University, ul. Astrakhanskaya 83, 410012 Saratov, Russia;
e-mail: zimnyakov@sgu.ru;
O.V. Ushakova Saratov State Technical University, ul. Politekhnicheskaya 77, 410071 Saratov, Russia;
R. Myllylä Department of Electrical Information Engineering, Optoelectronics and Measurement Techniques Laboratory, University of Oulu, P.O. Box 4500, 90014 University of Oulu, Finland;
e-mail: rist.myllyla@e.oulu.fi

Received 28 June 2006
Kvantovaya Elektronika **37** (1) 9 – 16 (2007)
Translated by M.N. Sapozhnikov

In this paper, we considered an alternative approach to the determination of the transport length in weakly absorbing random media, which is based on the analysis of the angular intensity distributions in coherent backscattering peaks taking into account the reflectivity of the layer boundaries. We studied dry paper layers and paper layers saturated with an immersion liquid representing a typical example of a random medium with fibrillar structure.

The propagation of probe radiation in dry paper layers is mainly determined by multiple scattering of light from structural elements of the paper (cellulose fibres, whose random network forms the paper structure, fragments of fibres and filler particles added to paper to impart the required properties to it). A high packing density and rather high refractive indices of scattering centres (~ 1.55 for cellulose fibres and from 1.52 to 2.5 for filler particles depending on their type; the value ~ 2.5 belongs to titanium dioxide particles) along with relatively weak absorption (for uncoloured paper) in the visible region give the optical density $\tau \approx \mu_s W = W/l$, which greatly exceeds unity even for samples of thickness 80 – 100 μm. This results in the predominantly diffusion regime of light propagation in dry paper layers and allows one to study their optical properties by optical diffusion methods (with some assumptions) and, hence, to use the models of radiation transfer based on the diffusion approximation. A typical example is the use of the Kubelka – Munk model to interpret the results of optical diagnostics of paper layers [7, 8]. The diffusion approximation can be also applied to analyse the data of paper sample probing obtained by pulsed-modulation methods and methods of low-coherence interferometry (in particular, time-of-flight photometry and optical coherence tomography), which are quire sensitive to variations in the structural characteristics of samples [9 – 11].

An important problem of optical diagnostics of multiply scattering media with a complex structure (in particular, paper) is the establishment of a relation between diagnostic parameters obtained by one or another of the optical methods and the structural characteristics of a medium being probed. To solve this problem in the case of optical probing of paper, different random-medium models of paper were considered. In particular, a multilayer model taking into account the roughness of layer interfaces was proposed in [12]. The optical model of paper as an ensemble of randomly oriented dielectric cylinders was considered in [13].

Interest in the investigation of optical characteristics of paper is also explained by the fact that it was assumed earlier in the studies of these characteristics by the method of time-of-flight photometry [9] that the scattering anisotropy of probe radiation in paper layers is extremely high ($g \approx 0.94 - 0.97$); however, the ratio l^*/l characterising the scattering anisotropy of probe radiation was not directly estimated. The assumption about such a high anisotropy of scattered light in paper layers was based on values of g for cellulose fibres as a main structural component of paper estimated by using the Mie theory. At the same time, the presence of filler particles and fibre fragments in paper layers, which have considerably lower values of the diffraction parameter $\pi d/\lambda$ (d is the characteristic size of scatterers) than cellulose fibres, should reduce the effective scattering anisotropy parameter of paper samples as the system of scatterers of different types compared to the values presented in [9].

In this connection, to establish the type of light scattering in paper layers, we also studied, along with the measurements of angular intensity distributions in coherent backscattering peaks at different probe radiation wavelength, the spectral dependences of T_d, R_d and T_c in the visible region for dry paper samples and samples saturated with liquids. This allowed us to compare the data obtained by different optical diffusion methods and to establish a predominantly isotropic nature of scattering of probe radiation in paper layers (by comparing the experimental values of l^* and l obtained as the result of analysis).

2. Experimental method and results

We studied samples of copy paper manufactured by different producers, which differed insignificantly in width W and volume solid fraction f: B Ballet Classic multimedia application paper (Svetogorsk Joint-Stock Company, Russia), Universal Office writing paper (Paper plant, Kotlas, Russia), OfficeLine writing paper (Ekort, Russia), and Data Copy office paper (M-Real, Sweden). Before experiments, we measured W for all paper samples at ten different regions of each of the samples and averaged the data obtained. Measurements were performed with a Micron-02 instrument (a digital instrument for checking the terminal length standards with an inductive displacement transducer; the measurement limits were 0 – 200 μm and the instrumental error was ±0.2 %). The deformation of paper samples during measurements in the contact region of the tip of the inductive sensor of a Micron-02 instrument with a sample did not affect considerably the results of measurements, which follows implicitly from a comparison of the density ρ of samples calculated from the measured thickness, mass (determined by weighing on an analytical balance), and sample area with the corresponding values presented by manufacturers. According to our measurements, $\rho = (79.7 \pm 4.1)$ g m^{-2} for sample No. 1 (according to the manufacturer, 80 g m^{-2}), (67.6 ± 3.8) g m^{-2} for sample No. 2 (65 g m^{-2}), (62.6 ± 3.5) g m^{-2} for sample No. 3 (65 g m^{-2}), and (81.8 ± 4.2) g m^{-2} for sample No. 4 (80 g m^{-2}).

A systematic error of the sample thickness measurements caused by the action of the tip of the inductive sensor on a sample was insignificant due to a small measurement stress produced by the sensor spring (no more than 0.3 N) and a rather large radius of curvature of the contact surface of the tip (and, hence, a large contact area of the tip with a sample). The random component of the error of sample thickness measurements at a fixed point, determined from a series of ten readings of the Micron-02 device for the 0.9 significance level, did not exceed ~ 1 μm. A similar component, determined as a result of measurements performed at ten different points chosen randomly within a region of size 100×100 mm, did not exceed ±5 μm. The volume fractions of a solid phase were estimated from the differences of the measured densities of dry paper samples and samples saturated with water during at least 12 hours. We used as immersion liquids distilled water and glycerol ('Ukr-KhimResurs', the fraction of pure glycerol being no less than 94 %), which substantially differ both in the refractive indices (~ 1.33 for water and ~ 1.47 for glycerol) and in viscosity.

Preliminary studies showed that for the saturation time of liquid samples $t_{sat} \geqslant 7 - 10$ h (depending on a dry sample

density), the dependences $\rho(t_{sat})$ of the density on the saturation time for all the samples studied achieve the stationary value $\rho(t_{sat}) \approx$ const. Note that the sample thickness increases by 10 % – 15 % upon saturation with liquids (depending on the saturating liquid, dry sample density and thickness), which is probably caused by the swelling of cellulose fibres upon their hydration. The increase in the thickness of samples saturated with liquid was taken into account in the analysis of experimental results. Sample thicknesses and volume fractions of a solid phase in samples obtained in preliminary experiments are presented in Table 1.

Table 1. Thickness W of samples and volume fraction f of a solid phase in them.

Sample number	W/μm	f
1	94 ± 4.7	0.45 ± 0.02
2	80 ± 4	0.42 ± 0.02
3	60 ± 3	0.35 ± 0.018
4	90 ± 4.5	0.39 ± 0.02

We obtained the angular intensity distributions in coherent backscattering peaks for probe radiation wavelengths 633 and 532 nm and the diffuse transmission and reflection spectra for paper samples in the range from 450 to 800 nm. Figure 1 presents the scheme of the experimental setup for analysis of the angular intensity distributions in coherent backscattering peaks. The sources of linearly polarised probe radiation were a 633-nm, 5-mW GN-5P helium – neon laser (Plasma Research and Production Association) and a diode-pumped doubled 532-nm, 2-mW cw Nd : YAG laser. The pump radiation beam was expanded with a $50^{\times}$ telescopic system with an aperture – a spatial filter (the beam diameter at the telescopic system output was 20 mm) and was directed with the help of a beamsplitter on a sample located in the object focal plane of an objective – Fourier transformer with a focal distance of 80 mm. A polarisation filter placed in front of the objective separated the co-polarised component of probe radiation scattered by the sample (i.e. the linearly polarised component with the electric field directed along the electric field in the probe beam). The angular intensity distributions of backscattered radiation were recorded in the image focal plane with a 10-bit, 780×580 pixel VS-CTT-075-2001 CCD camera (the pixel size was 8.3×8.3 μm).

Figure 2a shows the typical intensity distribution in the focal plane of the objective – Fourier transformer corresponding to the coherent backscattering peak observed upon probing of dry paper sample No. 1 with radiation at 633 nm, and Fig. 2b presents the corresponding shape of this peak. The half-widths $\Omega_{0.5}$ of coherent backscattering peaks were determined from the obtained angular intensity distributions $I(\theta)$ (Table 2). We did not measure the angular intensity distributions in coherent backscattering peaks at 532 nm for paper samples saturated with glycerol because of a poor quality of the peak images (in this case, low-order scattering of probe radiation occurred in samples, which suppressed coherent backward scattering).

We studied the diffuse transmission $[T_d(\lambda)]$ and reflection $[R_d(\lambda)]$ spectra of dry paper samples and samples saturated with immersion liquids in the range from 450 to 800 nm by using a Cary-2415 spectrophotometer equipped with an integrating sphere. Figure 3a presents spectra $T_d(\lambda)$ and $R_d(\lambda)$ for dry sample No. 1 and this sample saturated with immersion liquid (glycerol). To estimate the extinction coefficient $\mu_t = \mu_a + \mu_s$ of samples, we also measured their collimated transmission spectra $T_c(\lambda) \approx \exp(-\mu_t W)$ in the range from 400 to 800 nm by using an SDL-1 spectrometer equipped with a special collimating accessory consisting of three coaxial 1-mm apertures located in a cell department.

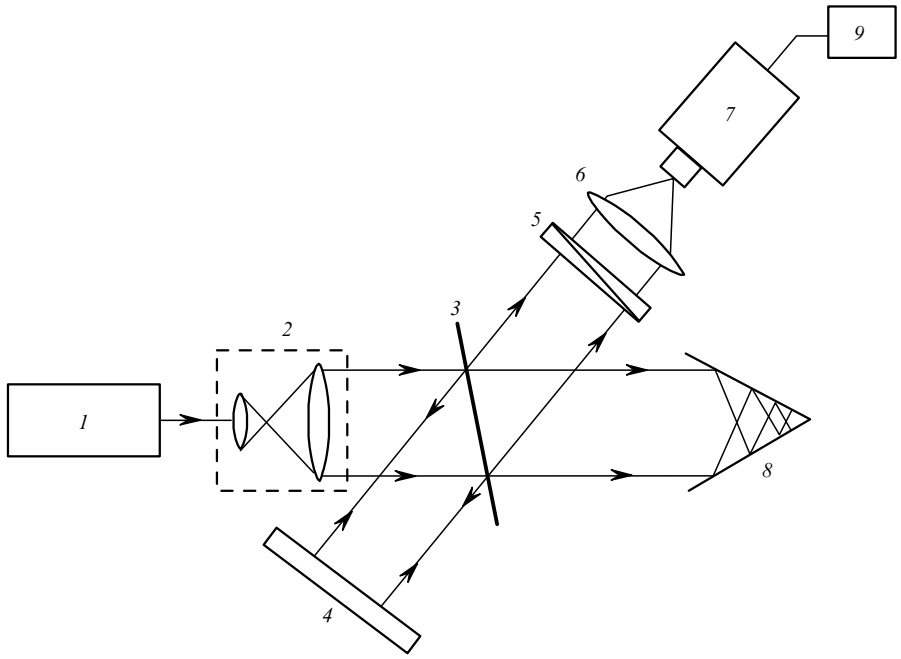

Figure 1. Scheme of the experimental setup for analysis of angular intensity distributions in coherent backscattering peaks: (*1*) laser (633 or 532 nm); (*2*) telescopic system consisting of a beam expander with a point diaphragm (spatial filter); (*3*) beamsplitter; (*4*) sample; (*5*) polariser; (*6*) objective – Fourier transformer; (*7*) CCD camera; (*8*) optical absorbing trap; (*9*) PC.

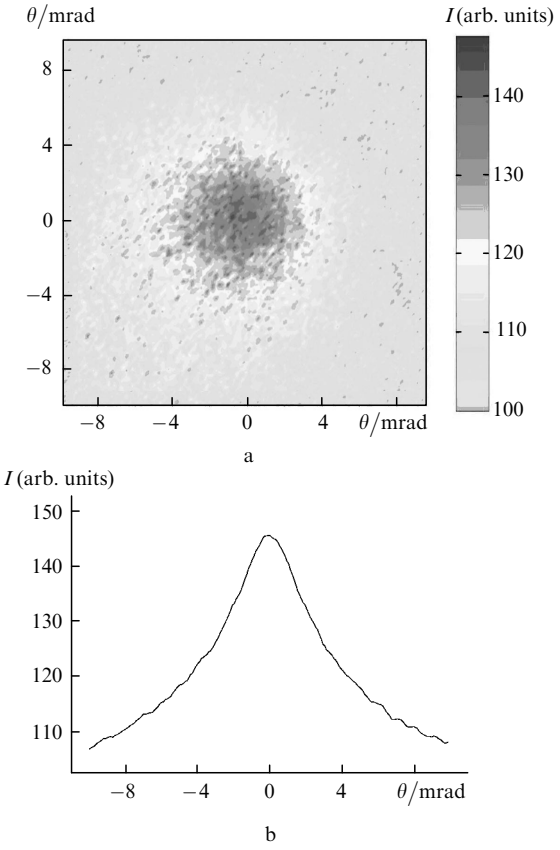

Figure 2. Typical angular intensity distribution in the coherent backscattered peak detected with a CCD camera (the coherence of radiation leads to a strong speckle modulation of detected radiation) (a) and the peak shape corresponding to the intensity distribution in Fig. 2a (speckles were suppressed by averaging the intensity distribution over 20 statistically independent speckle-modulated frames for a sample under study) (b).

Table 2. Peak half-width $\Omega_{0.5}$ (in mrad) for samples.

λ/nm	Sample number	Sample state		
		Dry	Saturated with water	Saturated with glycerol
633	1	6.2 ± 0.31	4.3 ± 0.22	3.5 ± 0.18
	2	6.16 ± 0.31	4.27 ± 0.21	3.6 ± 0.18
	3	6.7 ± 0.34	4.8 ± 0.24	4 ± 0.2
	4	6.3 ± 0.32	4.2 ± 0.21	4.5 ± 0.22
532	1	5.6 ± 0.28	3.7 ± 0.19	–
	2	5.2 ± 0.26	3.9 ± 0.19	–
	3	5.4 ± 0.27	3.3 ± 0.17	–
	4	5.2 ± 0.26	3.9 ± 0.2	–

The distance between the apertures was large enough (180 mm) to provide a negligible influence of forward-scattered radiation on the results of measurements compared to the influence of the unscattered (collimated) radiation component. Figure 3b shows the collimated transmission spectra obtained for dry and glycerol-saturated paper sample No. 3.

The propagation of probe radiation in visible and near-IR spectral regions in paper samples is mainly determined by scattering because $\mu_s \gg \mu_a$, and, hence, $\mu_t \approx \mu_s$. A preliminary analysis of our experimental results, performed

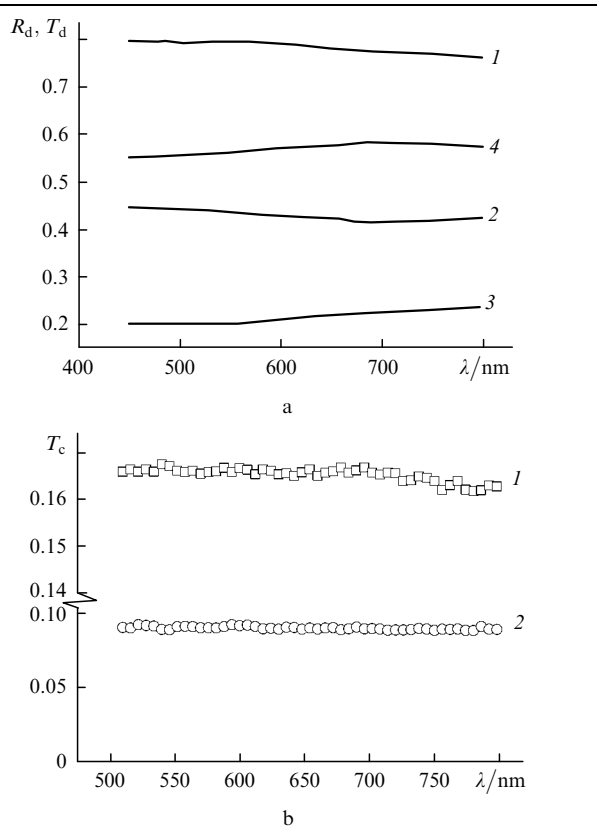

Figure 3. Diffusion reflection R_d (*1*, *2*) and transmission T_d (*3*, *4*) spectra for dry (*1*, *3*) and glycerol-saturated (*2*, *4*) sample No. 1 (a) and collimated transmission spectra for dry (*1*) and glycerol-saturated (*2*) sample No. 3 (b).

by neglecting the reflectivity of sample boundaries and their finite thickness in measurements of coherent backward scattering (in this case, the transport scattering coefficient is related to the half-width of the backward scattering peak by the approximate expression $\Omega_{0.5} \approx \lambda\mu_s'/(3\pi)$ [14]), suggests that in our case the relation $\mu_s \geqslant \mu_s'$ takes place (i.e. estimates of the scattering coefficient are comparable with those of the transport scattering coefficient, which means that the scattering of probe radiation has mainly the isotropic nature). This conclusion contradicts the assumption [9] about the essentially anisotropic nature of scattering of visible and near-IR radiation in dry paper layers ($g \simeq 0.94 - 0.98$ corresponds to the scattering regime with $\mu_s \gg \mu_s'$; in this case, the transport length in samples should considerably exceed their thickness).

The typical values (0.20 – 0.25) of diffuse transmission of dry paper samples in the visible and near-IR spectral regions obtained in our experiments contradict the assumption about the anisotropic nature of scattering for $l^* \gg W$. The transport length was also estimated by analysing the spatial intensity distributions of radiation scattered backward from the surface of a multilayer packet composed of paper samples upon the inclined incidence of a focused probe beam (the reflectometry method proposed by Wang and Jacques [15]). In the case of isotropic multiply scattering media, the transformation of the directed component of probe radiation to the diffusion component during the penetration of the probe beam to the medium leads to the eccentricity of the axially symmetric intensity distribu-

tions of diffusely scattered light, recorded with a CCD camera, with respect to the region of radiation input. The displacement of this region with respect to the geometric centre of the equal-intensity lines of diffusely scattered light is proportional in the first approximation to the transport length of the probed medium and depends on the effective refractive index of the medium and the angle of incidence of the probe beam.

Figure 4 shows the equal-intensity lines for diffusely scattered radiation at 633 nm for the angle of incidence of a focused probe beam equal to 35°. Small displacements (comparable with the pixel size of the CCD camera) of the geometrical centre of the equal-intensity lines of diffusely scattered light with respect to the region of incidence of probe radiation observed in experiments with the inclined incidence of the probe beam on a sample allow us to conclude that the transport length for dry paper samples lies in the interval between 10 and 25 μm (i.e. $l^* \ll W$).

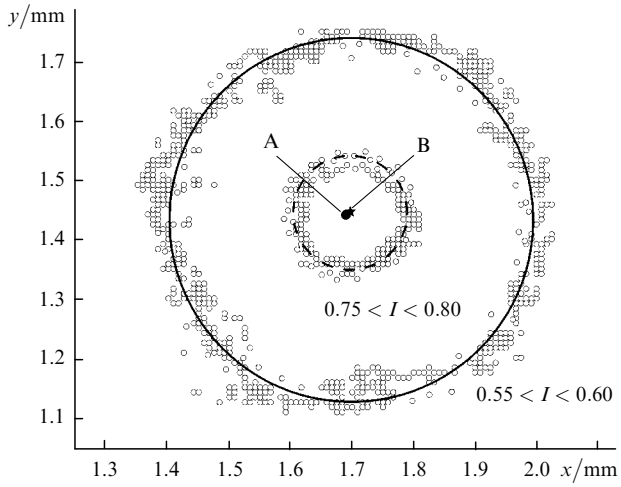

Figure 4. Equal-intensity lines for radiation diffusely scattered from a multilayer packet consisting of paper samples No. 2. The values presented in the figure are the ranges of normalised intensities chosen for the construction of the corresponding line (normalisation was performed to the value determined near the geometric centre of the distribution outside the radiation input region); point A corresponds to the centre of radiation input, point B corresponds to the geometrical centre of equal-intensity lines. A small eccentricity of the lines with respect to point A corresponds to a small transport length.

3. Analysis of experimental results

The shape and width of a coherent peak backscattered from a layer of a multiply scattering medium in the absence of absorption is determined not only by the transport length l^* but also by the ratio W/l^* and the reflectivity $\Re$ of the layer boundary. The value of $\Re$ depends in turn on the ratio of the effective refractive index $n_{\rm eff}$ of the layer to the refractive index $n_{\rm i}$ of a homogeneous medium from which the probe beam is incident on the layer boundary (in our case, $n_{\rm i} \approx 1$). Within the framework of diffusion approximation, the angular intensity distribution $I(\theta)$ in the coherent backscattering peak can be described by the expressions (see, for example, [16]):

$$I(\theta) = J(\theta) + J(0),$$

$$J(\theta) \equiv \frac{1}{2\pi l^{*3}} \int_0^W \mathrm{d}z_+ \int_0^W \mathrm{d}z_- \exp(-z_+/l^*) \exp(-z_-/l^*)$$

$$\times \int \mathrm{d}^2 r \exp(-\mathrm{i}rq) \sum_{n=-\infty}^{+\infty} \left[\frac{1}{(r^2 + a_n^2)^{1/2}} - \frac{1}{(r^2 + b_n^2)^{1/2}} \right], \quad (1)$$

where the cylindrical coordinate system rz is used for the axially symmetric case; $z_\pm$ are integration variables introduced in [16]; $q \equiv |\boldsymbol{k}_{\rm i} + \boldsymbol{k}_{\rm f}| = 2\pi\theta/\lambda$ is the modulus of the scattering vector; $\boldsymbol{k}_{\rm i}$ is the wave vector of the incident wave; $\boldsymbol{k}_{\rm f}$ is the wave vector of the detected scattered wave; $a_n = z_+ - z_- + 2n(W + 2z_{\rm b})$; $b_n = z_+ + z_- + 2z_{\rm b} + 2n(W + 2z_{\rm b})$; $z_{\rm b}$ is the extrapolation length measured from the layer boundary in the direction of negative values of z and determined by the condition that the diffusion component of scattered radiation is zero at a distance of $z_{\rm b}$ [17]. The value of $z_{\rm b}$ is determined by the reflectivity of the scattering layer reflectivity and, hence, by the effective refractive index $n_{\rm eff}$ of the scattering medium.

The boundary condition corresponding to the radiation transfer equation in the diffusion approximation obtained in [17] has the form

$$z_{\rm b} = \frac{2}{3} l^* \frac{1 + \Re}{1 - \Re}, \quad (2)$$

where the reflectivity $\Re$ of the layer boundary is found by integrating the reflection coefficient for nonpolarised light, calculated by using the Fresnel theory, over all possible angles of incidence of light on the boundary. Thus, $z_{\rm b}$ is a function of the effective refractive index of the scattering medium, which in turn affects the distribution $I(\theta)$ in the coherent scattering peak.

The results of intensity measurements of coherent backward scattering from paper samples were interpreted based on the method that was used earlier to analyse the transport characteristics of close-packed TiO_2 powder layers [18]. By using the half-widths $\Omega_{0.5}$ of coherent backscattering peaks measured in experiments, we plotted, according to (1) and (2), the dependences $l^* = \varphi(n_{\rm eff})$ corresponding to the measured values of $\Omega_{0.5}$. Figure 5 presents such dependences for one of the samples (both in the dry state and saturated with water or glycerol), which illustrate a considerable influence of the reflectivity of the layer boundary on the formation of the coherent backscattering peak. The values of $l^* = \varphi(n_{\rm eff})$ were calculated for specified $n_{\rm eff}$ taking into account a change in the thickness of samples (approximately by 10 % – 15 %) upon their saturation with immersion liquids. The effective refractive index for dry paper samples and samples saturated with immersion liquids was calculated by using the Maxwell – Garnett theory [5], according to which the average value of the relative dielectric constant of a two-component composite medium is

$$\bar{\varepsilon} = n_{\rm eff}^2 \approx \varepsilon_2 \left(1 + \frac{2f\alpha}{1 - f\alpha} \right), \quad (3)$$

where ε_2 is the relative dielectric constant of the base medium into which scattering centres consisting of a material with the relative dielectric constant ε_1 (in our case, cellulose fibres) are embedded; f is the volume fraction

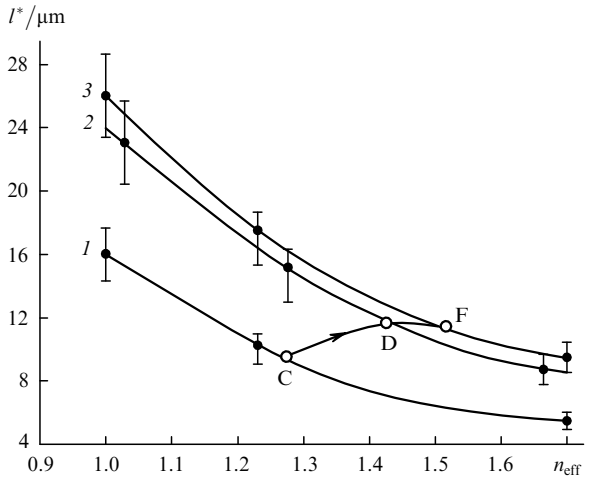

Figure 5. Dependences $l^* = \varphi(n_{eff})$ corresponding to the values of $\Omega_{0.5}$ measured for dry (*1*), water-saturated (*2*), and glycerol-saturated (*3*) sample No. 4 at the probe radiation wavelength of 633 nm. The line with the arrow illustrates variation in the optical parameters of the sample upon its saturation with immersion liquids (see Table 2). The confidence intervals correspond to the measurement errors for $\Omega_{0.5}$ and W.

of scattering centres; and $\alpha = (\varepsilon_1 - \varepsilon_2)/(\varepsilon_1 + \varepsilon_2)$ is the depolarisability factor. Although such an approach is limited due to a restriction imposed on the relation between the characteristic size of scattering centres and the probe radiation wavelength, in [19] satisfactory results were obtained even in by using the Maxwell–Garnett theory to calculate the optical parameters of random ensembles of dielectric cylinders of diameter comparable with the propagating radiation wavelength. The values of n_{eff} were estimated for dry paper samples and samples saturated with immersion liquids by assuming that $\varepsilon_1 = n_1^2 = n_{cel}^2 \approx 2.40$ (cellulose), $\varepsilon_2 = 1$ (dry samples), $\varepsilon_2 = n_{H_2O}^2 \approx 1.77$ (samples saturated with water), $\varepsilon_2 = n_{Gl}^2 \approx 2.16$ (samples saturated with glycerol).

The curve with the arrow in Fig. 5 demonstrates the change in the effective refractive index n_{eff} and transport length l^* obtained from the experimental data upon saturation of the probed medium with water and glycerol. A considerable increase in the transport length (and, hence, a decrease in the transport scattering coefficient) with increasing n_{eff} is caused by the trivial immersion effect (optical clearing of the probed medium) due to a decrease in the ratio $\varepsilon_1/\varepsilon_2$ and lowering the efficiency of scattering of probe radiation by scattering centres (cellulose fibres).

The diffuse transmission of dry paper samples (for which $W \gg l^*$) measured in our experiments was interpreted by using the known relation for the diffuse transmission of a layer, which was obtained within the framework of the diffusion approximation of the radiation transfer theory (see, for example, [20, 21]):

$$T_d(W) = \frac{l^* + z_{b1}}{W + z_{b1} + z_{b2}}, \quad (4)$$

where z_{b1} and z_{b2} are the extrapolation lengths for the first and second boundaries of the layer, respectively (in our case, $z_{b1} = z_{b2}$). Estimates of the transport length for dry samples according to (4) are in good agreement with these lengths obtained by analysing the measurements of the intensity $I(\theta)$ in coherent backscattering peaks. The discrepancy between the transport lengths estimated by these two methods does not exceed 15 % (for example, the value of l^* for sample No. 4 obtained by analysing the measurements of $I(\theta)$ at 633 nm is (9.6 ± 1.0) μm, whereas the value of l^* estimated from diffuse transmission according to (4) is (10.8 ± 0.9) μm.

Table 3. Transport length l^* determined from intensity measurements of coherent backscattering peaks and scattering length l determined from collimated transmission measurements.

Sample number	Sample state	$\lambda = 633$ nm			$\lambda = 532$ nm		
		$l^*/\mu m$	$l/\mu m$	l^*/l	$l^*/\mu m$	$l/\mu m$	l^*/l
1	Dry	9.2 ± 1.0	7.6 ± 0.8	~ 1.21	6.9 ± 0.8	7.5 ± 0.8	~ 0.92
	Saturated with water	12.5 ± 1.3	9.7 ± 0.1	~ 1.29	8.0 ± 0.8	9.5 ± 0.1	~ 0.84
	Saturated with glycerol	13.9 ± 1.4	11.0 ± 1.1	~ 1.26	–	–	–
2	Dry	10.0 ± 1.1	6.2 ± 0.6	~ 1.61	7.0 ± 0.8	6.1 ± 0.6	~ 1.15
	Saturated with water	15.1 ± 1.5	7.7 ± 0.8	~ 1.96	7.4 ± 0.8	7.6 ± 0.8	~ 0.97
	Saturated with glycerol	15.3 ± 1.5	8.4 ± 0.8	~ 1.82	–	–	–
3	Dry	11.0 ± 1.2	5.8 ± 0.6	~ 1.9	8.7 ± 0.9	5.8 ± 0.6	~ 1.5
	Saturated with water	13.9 ± 1.4	6.4 ± 0.6	~ 2.17	11.0 ± 1.2	6.4 ± 0.6	~ 1.7
	Saturated with glycerol	14.5 ± 1.5	7.2 ± 0.7	~ 2.01	–	–	–
4	Dry	9.6 ± 1.0 (point C in Fig. 5)	6.9 ± 0.7	~ 1.39	9.5 ± 1.0	7.2 ± 0.7	~ 1.32
	Saturated with water	11.3 ± 1.2 (point D in Fig. 5)	8.4 ± 0.8	~ 1.35	10.1 ± 1.1	8.5 ± 0.9	~ 1.19
	Saturated with glycerol	11.4 ± 1.2 (point F in Fig. 5)	8.9 ± 0.9	~ 1.28	–	–	–

Note that the data obtained from analysis of the angular intensity distributions and diffuse transmission of dry paper samples demonstrate that l^* decreases with decreasing wavelength, whereas the collimated transmission spectra show that the extinction coefficient is constant in the visible region (see Fig. 3b), which corresponds to a decrease in the ratio l^*/l in the short-wavelength region of the visible spectral range.

Table 3 presents the transport lengths obtained from the angular intensity distributions $I(\theta)$, and scattering lengths found from the measurements of collimated transmission at the corresponding wavelengths. These results demonstrate the isotropic nature of probe radiation scattering in paper samples.

4. Conclusions

We have considered the method for interpretation of experimental data on diffuse scattering of light (in particular, measurements of the angular intensity distributions in coherent backscattering peaks) in random media with close-packed scattering centres. The method can be used to estimate the transport coefficient of a probed medium taking into account the influence of the reflectivity of the probed medium – free space interface, caused by multiple reflections of the partial components of the scattered light field from the boundary in the medium, on the diffuse of radiation in the medium layer. The method is based on the one-to-one correspondence between the half-width of the coherent backward scattering peak measured in experiments and the values of the effective refractive index n_{eff} and transport length l^* for the probed medium. The values of n_{eff} were estimated for the specified structural properties of the probed medium (in particular, the volume fraction of scattering centres) by using the Maxwell – Garnett model.

The effective refractive index can be also determined by analysing the experimental angular intensity distribution of radiation diffusely scattered in a medium, as proposed in [22]. The model of the effective medium can be also used (for example, based on the coherent potential approximation [19, 23]) to find n_{eff} for a probed medium by using its structural parameters. Transport lengths for dry paper samples and samples saturated with immersion liquids obtained by measuring the intensities of coherent backward scattering peaks by this method are in good agreement with the values obtained by measuring diffuse transmission.

It is important to know the influence of the coherence length of radiation sources used in experiments on the measurements of the coherent backscattering peak intensity. We have measured the coherence lengths for lasers employed in our experiments (by using a Michelson interferometer), which were ~ 14 cm (for a helium – neon laser and ~ 1.9 mm for a diode-pumped Nd : YAG laser). Both these values greatly exceed the maximum values of the transport length and thickness of paper samples, so that the influence of the radiation coherence length on the measurements can be neglected.

Our experiments have shown that scattering of radiation in paper samples has the isotropic nature ($l^* \geqslant l$, which follows from a comparison of the results of measurements of the intensities of coherent backward scattering peaks, diffuse and collimated transmission). This conclusion contradicts the assumption [9] that light scattering in paper samples has the anisotropic nature. Note that a main structural element of paper is cellulose fibres of diameter $d \approx 10 - 20$ μm. For isolated cylindrical scatterers characterised by rather large diffraction parameters $\pi d/\lambda$ in the visible region ($\sim 50 - 150$), light scattering anisotropy indeed should be observed in the direction perpendicular to the axes of cylinders, which was the reason for the assumption made in [9].

At the same time, the diffuse propagation of radiation in paper layers also considerably depends on other components of paper, which have much smaller dimensions (in particular, submicron filler particles used to provide the required quality of paper). In addition, in the case of a rather large volume fraction of scattering centres in a medium, the 'inversion' effect is possible, when the role of the base medium into which scatterers are embedded is played not by air or immersion liquid filling the space between scatterers but the material of scattering centres into which microscopic volumes of air or liquid are embedded. Also, it is necessary to take into account the microscopic structure of cellulose fibres, which are not homogeneous cylindrical scattering centres.

Acknowledgements. The authors thank V.I. Kochubei for his help in spectral measurements. This work was supported by the Russian Foundation for Basic Research (Grant No. 04-02-16533) and a grant of AFGIR and the Ministry of Education of the Russian Federation 'Mezooptika' [Analytical Departmental Program 'Development of the Scientific Potential of the Higher School (2006 – 2008)', Project code RNP.2.1.14473].

References

1. Ishimaru A. *Wave Propagation and Scattering in Random Media* (New York: Acad. Press, 1978).
2. Chandrasekhar S. *Radiative Transfer* (New York: Dover, 1960).
3. Salnier P.M., Zinkin M.P., Watson G.H. *Phys. Rev. B*, **42**, 2621 (1990).
4. Shinde R., Baldi G., Richter S., et al. *Appl. Opt.*, **38**, 197 (1999).
5. Bohren C.F., Huffman D.R. *Absorption and Scattering of Light by Small Particles* (New York: Wiley, 1983; Moscow: Mir, 1986).
6. Tuchin V.V. *Lazery i volokonnaya optika v biomeditsinskikh issledovaniyakh* (Lasers and Fibre Optics in Biomedical Studies) (Saratov: Saratov State University, 1998).
7. Niskanen K. *Paper Physics, Papermaking Science and Technology* (Jyväskylä: Fapet Oy, 1998) Vol. 16.
8. Borch J. et al. *Handbook of Physical Testing of Paper* (New York: Marcel Dekker, 2002) Vol. 2.
9. Carlsson J., Hellentin P., Malmqvist L., Persson A., Persson W., Wahlstrom C.-G. *Appl. Opt.*, **34**, 1528 (1995).
10. Alarousu E., Krehut L., Myllylä R., Hast J. *Proc. SPIE Int. Soc. Opt. Eng.*, **5475**, 48 (2004).
11. Alarousu E., Krehut L., Prykäri T., Myllylä R. *Meas. Sci. Technol.*, **16**, 1131 (2005).
12. Kirillin M.Yu., Priezzhev A.V., Hast J., Myllylä R. *Kvantovaya Elektron.*, **36**, 174 (2006) [*Quantum Electron.*, **36**, 174 (2006)].
13. Green K., Lamberg L., Lumme K. *Appl. Opt.*, **39**, 4669 (2000).
14. Kim Y.L., Liu Y., Turzhitsky V.M., Roy H.K., Wali R.K., Backman V. *Opt. Lett.*, **29** (16), 1906 (2004).
15. Wang L., Jacques S. *Appl. Opt.*, **34**, 2362 (1995).
16. MacKintosh F.C., John S. *Phys. Rev. B*, **37**, 1884 (1988).
17. Zhu J.X., Pine D.J., Weitz D.A. *Phys. Rev. A*, **44**, 3948 (1991).
18. Zimnyakov D.A., Kuznetsova L.V., Pravdin A.B. *Pis'ma Zh. Eksp. Teor. Fiz.*, **82**, 300 (2005).
19. Kirchner A., Busch K., Soukoulis C.M. *Phys. Rev. B*, **57**, 277 (1998).

20. Rivas J.G., Sprik R., Soukoulis C.M., Busch K., Lagendijk A. *Europhys. Lett.*, **48**, 22 (1999).
21. Rivas J.G., Sprik R., Lagendijk A., Noordam L.D., Rella C.W. *Phys. Rev. E*, **63**, 046613 (2001).
22. Rivas J.G., Dau D.H., Imhof A., Sprik R., Bret B.P.J., Johnson P.M., Hijmans T.W., Lagendijk A. *Opt. Comm.*, **220**, 17 (2003).
23. Busch K., Soukoulis C.M. *Phys. Rev. E*, **54**, 893 (1996).